Ablation of $\alpha_2\delta$-1 inhibits cell-surface trafficking of endogenous N-type calcium channels in the pain pathway in vivo

Manuela Nieto-Rostro[a,1], Krishma Ramgoolam[a,1], Wendy S. Pratt[a], Akos Kulik[b,c], and Annette C. Dolphin[a,2]

[a]Department of Neuroscience, Physiology and Pharmacology, University College London, WC1E 6BT London, United Kingdom; [b]Institute of Physiology II, Faculty of Medicine, University of Freiburg, 79104 Freiburg, Germany; and [c]BIOSS Centre for Biological Signalling Studies, University of Freiburg, 79104 Freiburg, Germany

Edited by Richard W. Tsien, NYU Neuroscience Institute, New York, NY, and approved October 19, 2018 (received for review June 30, 2018)

The auxiliary $\alpha_2\delta$ calcium channel subunits play key roles in voltage-gated calcium channel function. Independent of this, $\alpha_2\delta$-1 has also been suggested to be important for synaptogenesis. Using an epitope-tagged knockin mouse strategy, we examined the effect of $\alpha_2\delta$-1 on $Ca_V2.2$ localization in the pain pathway in vivo, where $Ca_V2.2$ is important for nociceptive transmission and $\alpha_2\delta$-1 plays a critical role in neuropathic pain. We find $Ca_V2.2$ is preferentially expressed on the plasma membrane of calcitonin gene-related peptide-positive small nociceptors. This is paralleled by strong presynaptic expression of $Ca_V2.2$ in the superficial spinal cord dorsal horn. EM-immunogold localization shows $Ca_V2.2$ predominantly in active zones of glomerular primary afferent terminals. Genetic ablation of $\alpha_2\delta$-1 abolishes $Ca_V2.2$ cell-surface expression in dorsal root ganglion neurons and dramatically reduces dorsal horn expression. There was no effect of $\alpha_2\delta$-1 knockout on other dorsal horn pre- and postsynaptic markers, indicating the primary afferent pathways are not otherwise affected by $\alpha_2\delta$-1 ablation.

calcium channel | primary afferent | auxiliary subunit | N-type | trafficking

The neuronal N-type voltage-gated calcium channel was first identified in primary afferent dorsal root ganglion (DRG) neurons (1, 2). Toxins from the *Conus* marine snails, ω-conotoxin GVIA and ω-conotoxin MVIIC, are highly selective blockers of N-type channels (3, 4) and have been instrumental in dissecting their function (5, 6). A key role for N-type calcium channels was identified in primary afferent neurotransmission in the dorsal horn of the spinal cord, and these toxins were therefore pursued as a therapeutic target in the alleviation of chronic pain (7, 8). Indeed, the peptide ziconotide (synthetic ω-conotoxin MVIIA) is licensed for intrathecal use in intractable pain conditions (9, 10).

Despite the functional importance of N-type channels in the pain pathway, a major hindrance to the study of their distribution and trafficking, in this system and elsewhere, has been the paucity of antibodies recognizing this channel. Although previous studies have used anti-peptide antibodies to intracellular $Ca_V2.2$ epitopes (for example, refs. 11 and 12), these have not shown plasma membrane localization of the endogenous channel in neurons and have not been rigorously examined against knockout tissue. For this reason, we developed a $Ca_V2.2$ construct with an exofacial epitope tag to detect its cell-surface expression and trafficking (13). This channel is observed on the plasma membrane, when expressed in DRGs and other neurons (13–15). We took advantage of our finding that the presence of the epitope tag did not affect function (13) to generate a knockin (KI) mouse line containing the hemagglutinin (HA) tag in the same position in the *Cacna1b* gene. This has allowed us to examine the distribution of native $Ca_V2.2$ protein in the intact nervous system.

N-type calcium channels are made up of the $Ca_V2.2$ pore-forming α1-subunit, which associates with auxiliary $\alpha_2\delta$- and β-subunits (16). Many studies have indicated that $\alpha_2\delta$-subunits are important for the correct trafficking and physiological function of the channels (for a review, see ref. 17). A significant role for $\alpha_2\delta$-1 in chronic neuropathic pain, which results from damage to peripheral sensory nerves, was identified as a result of two advances. First, it was shown that $\alpha_2\delta$-1 mRNA and protein are strongly up-regulated in somatosensory neurons following nerve damage (18–20). Second, $\alpha_2\delta$-1 was identified as the therapeutic target for the drugs gabapentin and pregabalin, which are used in neuropathic pain such as postherpetic neuralgia (21, 22). Furthermore, $\alpha_2\delta$-1 overexpression in mice resulted in a chronic pain-like phenotype (23), whereas knockout of $\alpha_2\delta$-1 caused a marked delay in the development of neuropathic mechanical hypersensitivity (24). However, it has not yet been possible to examine the effect of $\alpha_2\delta$-1 on the trafficking of the relevant N-type channels in vivo.

Here we elucidate the cellular and subcellular localization of native $Ca_V2.2$ in neurons of the peripheral somatosensory nervous system. We reveal a dramatic effect of $\alpha_2\delta$-1 ablation on $Ca_V2.2$ distribution, particularly in a key subset of nociceptive sensory neurons. In contrast to an early study of the subunit composition of N-type channels (16), which showed an ∼1:1 stoichiometry with $\alpha_2\delta$-1, a more recent study suggested that $\alpha_2\delta$-subunits were only associated with less than 10% of digitonin-solubilized Ca_V2 channels (25), although it cannot be ruled out that they became dissociated during solubilization. However, the present study reinforces the essential nature of the auxiliary

Significance

Neuronal N-type ($Ca_V2.2$) voltage-gated calcium channels are important at the first synapse in the pain pathway. In this study, we have characterized a knockin mouse containing $Ca_V2.2$ with an extracellular HA tag to determine the localization of $Ca_V2.2$ in primary afferent pain pathways. These endogenous channels have been visualized at the plasma membrane and rigorously quantified in vivo. We examined the effect of ablation of the calcium channel auxiliary subunit $\alpha_2\delta$-1 (the target of gabapentinoids) on $Ca_V2.2$ distribution. We found preferential cell-surface localization of $Ca_V2.2$ in DRG nociceptor neuron cell bodies was lost, accompanied by a dramatic reduction at dorsal horn terminals, but no effect on distribution of other spinal cord synaptic markers.

Author contributions: M.N.-R., K.R., W.S.P., and A.C.D. designed research; M.N.-R., K.R., and A.K. performed research; M.N.-R. contributed new reagents/analytic tools; M.N.-R., K.R., and A.C.D. analyzed data; and M.N.-R., K.R., A.K., and A.C.D. wrote the paper.

The authors declare no conflict of interest.

This article is a PNAS Direct Submission.

See Commentary on page 12848.

[1]M.N.-R. and K.R. contributed equally to this work.

[2]To whom correspondence should be addressed. Email: a.dolphin@ucl.ac.uk.

This article contains supporting information online at www.pnas.org/lookup/suppl/doi:10.1073/pnas.1811212115/-/DCSupplemental.

Published online November 28, 2018.

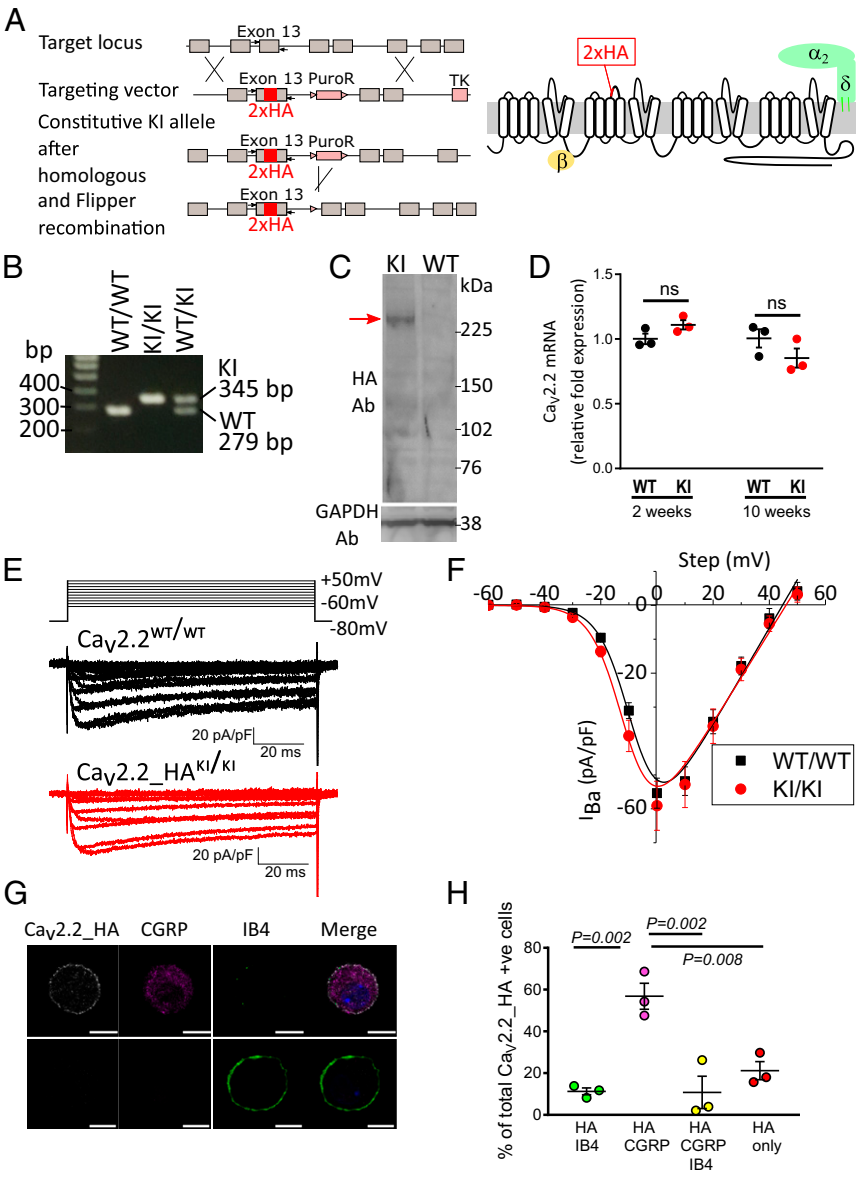

Fig. 1. Characterization of $Ca_V2.2$_HA knockin mice. (*A*, *Left*) Strategy for generation of $Ca_V2.2\_HA^{KI/KI}$ mice. (*A*, *Right*) Diagram of $Ca_V2.2$ showing the position of the HA tag. (*B*) Genotyping showing PCR product size for $Ca_V2.2^{WT/WT}$, $Ca_V2.2\_HA^{KI/KI}$, and $Ca_V2.2\_HA^{KI/WT}$ mice, using the primers shown in *A*. (*C*) Immunoblot of spinal cord synaptosomes from $Ca_V2.2\_HA^{KI/KI}$ mice (*Left*) and $Ca_V2.2^{WT/WT}$ mice (*Right*), confirming expression of $Ca_V2.2$_HA at the expected size (red arrow). GAPDH (*Lower*) is the loading control. Representative of three independent experiments from different mice. The molecular mass of $Ca_V2.2$_HA is 261.0 ± 1.2 kDa. (*D*) qPCR for $Ca_V2.2$ mRNA in brains from $Ca_V2.2\_HA^{KI/KI}$ (red circles), compared with $Ca_V2.2^{WT/WT}$ (black circles), at 2 and 10 wk postnatally (n = 3 mice per condition, each assayed in triplicate; one outlier triplicate value was omitted). Mean ± SEM is also shown. ns, not significant, paired t test. (*E*) Representative calcium channel currents recorded from $Ca_V2.2^{WT/WT}$ (black traces) and $Ca_V2.2\_HA^{KI/KI}$ (red traces) DRG neurons in culture (1 d in vitro). Currents were recorded at 10-mV intervals from −60 to + 50 mV. Capacitance transients have been cropped. (*F*) Current–voltage (IV) relationships (mean ± SEM) for I_{Ba} from $Ca_V2.2\_HA^{KI/KI}$ (red circles; n = 39 cells from four mice) and $Ca_V2.2^{WT/WT}$ (black squares; n = 37 cells from four mice) DRG neurons. Data were fit with a modified Boltzmann relationship (*SI Appendix, Methods*). For $Ca_V2.2\_HA^{KI/KI}$ and $Ca_V2.2\_HA^{WT/WT}$, the parameters for the illustrated fits are $V_{50,act}$ −10.69 and −8.00 mV; G_{max} 1.34 and 1.42 nS.pF^{-1}; and V_{rev} +45.9 and +44.7 mV, respectively. For the individual data for $Ca_V2.2\_HA^{KI/KI}$ (n = 39) and $Ca_V2.2\_HA^{WT/WT}$ (n = 37), $V_{50,act}$ was −9.87 ± 0.62 and −8.30 ± 0.48 mV; G_{max} was 1.31 ± 0.15 and 1.43 ± 0.09 nS.pF^{-1}; and V_{rev} was +44.0 ± 1.5 and +44.3 ± 1.5 mV, respectively. None of the parameters show any statistical difference (Student's t test). (*G*) Images of cultured DRG neurons from $Ca_V2.2\_HA^{KI/KI}$ mice showing (*Left* to *Right*) $Ca_V2.2$_HA staining before permeabilization, CGRP staining following permeabilization, IB4-FITC, and merged for two representative CGRP-positive (*Top*) and IB4-positive (*Bottom*) cells. (Scale bars: 10 μm.) (*H*) Quantification of the percentage of cells with cell-surface $Ca_V2.2$_HA that were also positive for IB4 (green circles), CGRP (lilac circles), CGRP and IB4 (yellow circles), or neither marker (red circles). Individual data points represent the mean data from three separate experiments and a total of 206 DRG neurons. Mean ± SEM of the three experiments is superimposed. Statistical significances compared with HA + CGRP-containing DRG neurons are shown (one-way ANOVA and Sidak's multiple-comparisons test).

$\alpha_2\delta$-1 protein for cell-surface expression of endogenous $Ca_V2.2$, both in DRG neuronal cell bodies and in their presynaptic terminals. No effect of $\alpha_2\delta$-1 loss was observed on other pre- and postsynaptic markers in the dorsal horn, despite a previous study implicating postsynaptic $\alpha_2\delta$-1 in thrombospondin-mediated synaptogenesis (26). Our results therefore show that loss of synaptic $Ca_V2.2$ as a result of $\alpha_2\delta$-1 ablation is due to a reduction of $Ca_V2.2$ trafficking to synapses, rather than synapse loss.

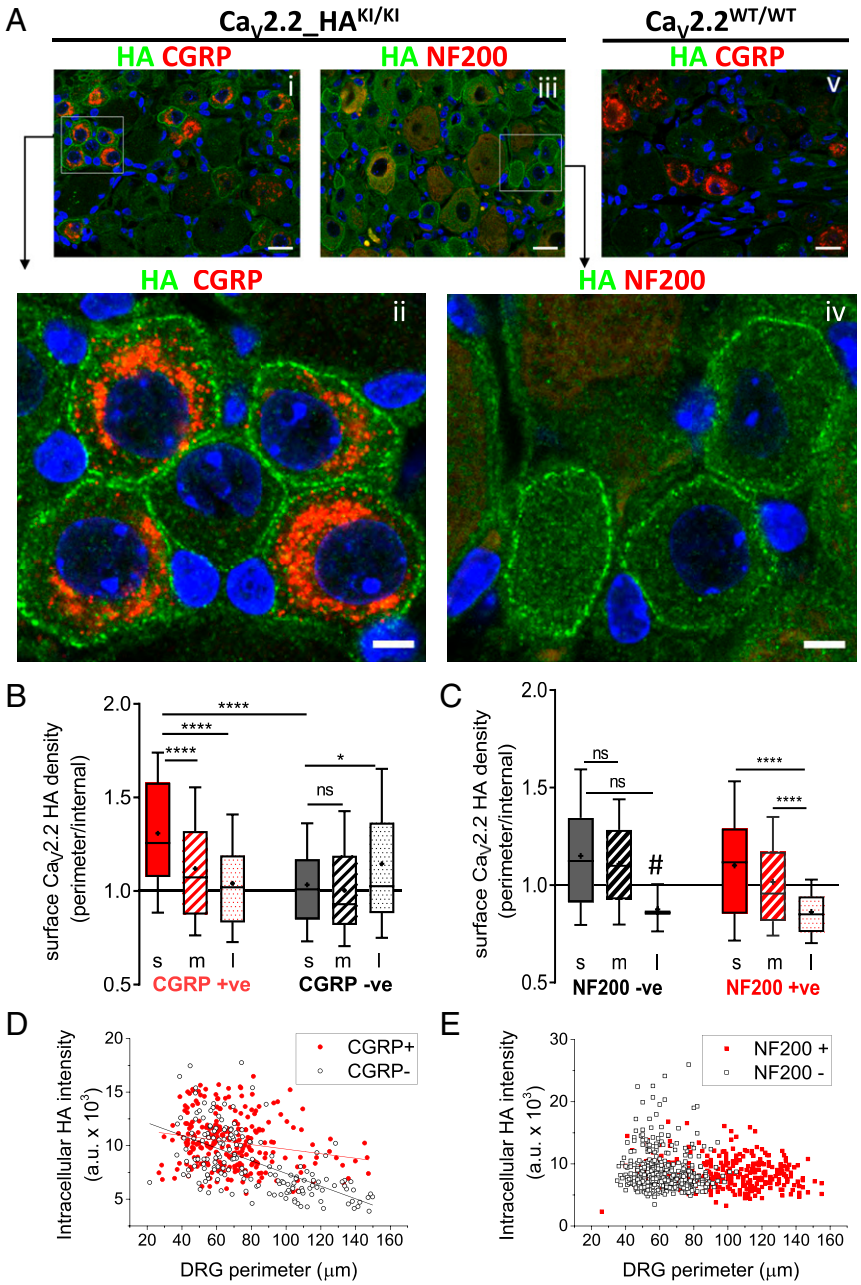

Fig. 2. Distribution of $Ca_V2.2\_HA$ in intact dorsal root ganglia. (*A*) Immunostaining for HA (green) in $Ca_V2.2\_HA^{KI/KI}$ (*i–iv*) and WT DRG neurons (*v*), costained with CGRP (*i*, *ii*, and *v*) or NF200 (*iii* and *iv*) (red). Nuclei are stained with DAPI (blue). Images *ii* and *iv* are enlargements of the ROIs shown in *i* and *iii*. [Scale bars: 20 (*i*, *iii*, and *v*) and 5 μm (*ii* and *iv*).] Lack of HA staining in $Ca_V2.2^{WT/WT}$ sections (*v*) was observed in four additional independent experiments. (*B*) Surface $Ca_V2.2\_HA$ intensity measured as a ratio of DRG neuronal perimeter/cytoplasmic staining for small (s; solid bars), medium (m; hatched bars), and large (l; shaded bars) DRG neurons that are either CGRP-positive (red) or CGRP-negative (black/dark gray). $n = 313$, 341, 122, 171, 169, and 164 DRG neurons, respectively, from sections from at least three mice. $^{****}P < 0.0001$, $^{*}P = 0.0135$ (one-way ANOVA and Sidak's post hoc test of all conditions with correction for multiple comparisons); ns, not significant. (*C*) Surface $Ca_V2.2\_HA$ intensity measured as a ratio of DRG neuronal perimeter/cytoplasmic staining for small, medium, and large DRG neurons that are either NF200-negative (black) or NF200-positive (red). $n = 213$, 201, 3, 36, 97, and 192 DRG neurons, respectively, from sections from at least three mice. #: Note very few large DRG neurons are NF200-negative. $^{****}P < 0.0001$ (one-way ANOVA and Sidak's post hoc test of all conditions with correction for multiple comparisons); ns, not significant. (*D* and *E*) Intracellular $Ca_V2.2\_HA$ staining, quantified with respect to cell size, for CGRP-positive (red circles) and CGRP-negative (open black circles) DRG neurons (*D*), and for NF200-positive (red squares) and NF200-negative (open black squares) DRG neurons (*E*). Data are from a subset of experiments from *B* performed in parallel in which the absolute immunostaining levels are directly comparable. Linear regression analysis for data in *D* (red line, CGRP +ve: slope −21.2, $r^2 = 03989$, *df* 260, $F = 10.8$, $P = 0.0012$; black line, CGRP −ve: slope −59.2, $r^2 = 0.362$, *df* 168, $F = 95.3$, $P < 0.0001$).

Results

Generation of $Ca_V2.2\_HA$ Knockin Mice. Mice containing a double-HA tag in constitutive exon 13 of the *Cacna1b* gene were generated in a C57BL/6 background, as described in *Methods*, such that every endogenous $Ca_V2.2$ contained the double-HA tag in the position previously ascertained not to affect channel function (13) (Fig. 1*A*). The presence of the HA tag was confirmed by PCR (Fig. 1*B*). We confirmed that the HA-tagged $Ca_V2.2$ protein is expressed in synaptosomes, since a 261-kDa band (the expected molecular mass of

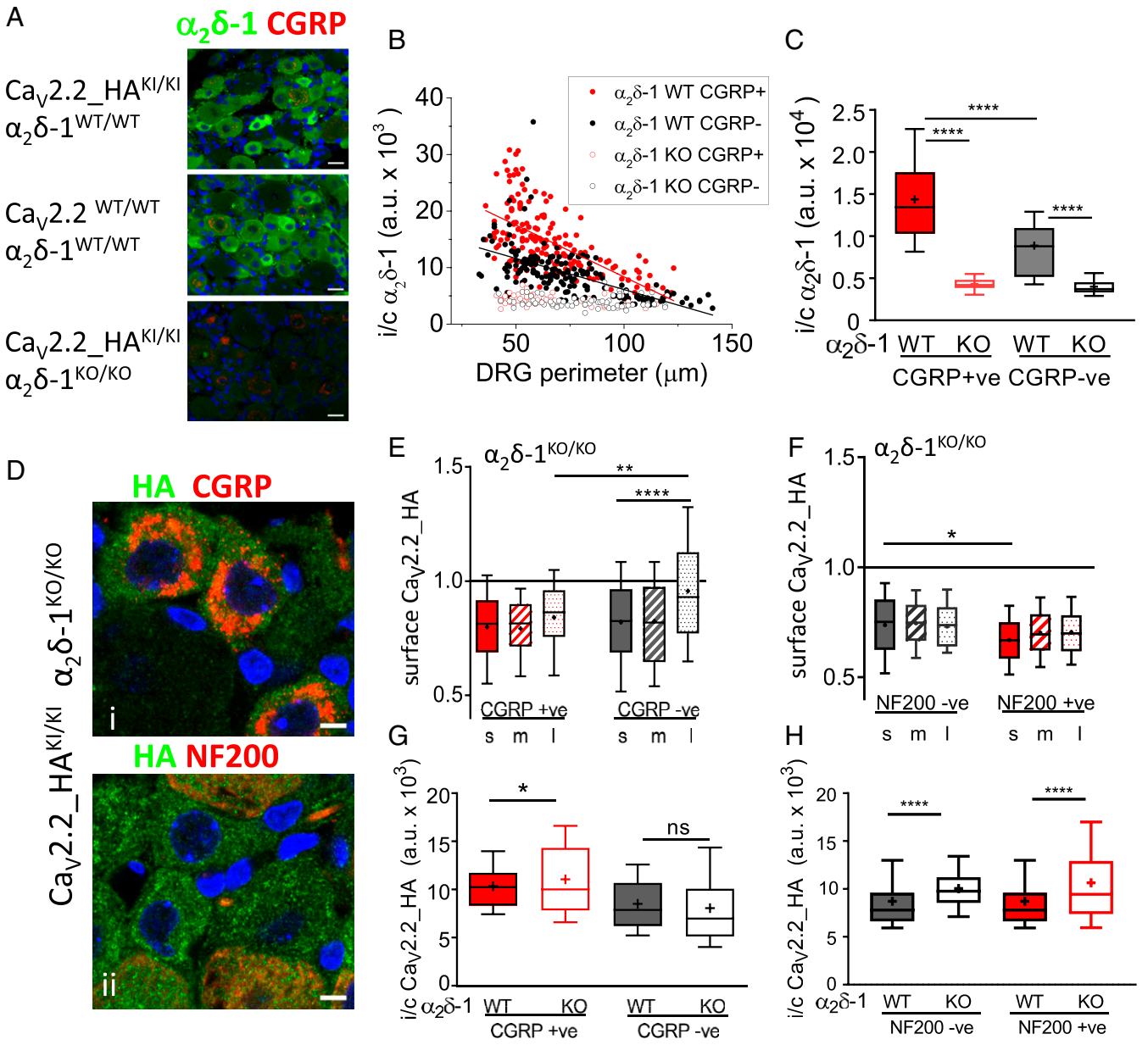

Fig. 3. Effect of $\alpha_2\delta$-1 ablation on distribution of $Ca_V2.2$_HA in intact dorsal root ganglia. (*A*) Immunostaining for $\alpha_2\delta$-1 (green) in $Ca_V2.2\_HA^{KI/KI}$ $\alpha_2\delta$-$1^{WT/WT}$ (*Top*), $Ca_V2.2^{WT/WT}$ $\alpha_2\delta$-$1^{WT/WT}$ (*Middle*), and $Ca_V2.2\_HA^{KI/KI}$ $\alpha_2\delta$-$1^{KO/KO}$ (*Bottom*) DRG sections, costained with CGRP (red). Nuclei were stained with DAPI (blue). (Scale bars: 20 μm.) (*B*) Intracellular (i/c) $\alpha_2\delta$-1 density with respect to cell size, for CGRP-positive (red circles) and CGRP-negative (black circles) DRG neurons from $Ca_V2.2\_HA^{KI/KI}$ $\alpha_2\delta$-$1^{WT/WT}$ (solid circles) and $Ca_V2.2\_HA^{KI/KI}$ $\alpha_2\delta$-$1^{KO/KO}$ (open circles) mice. Lines are linear fits for both CGRP-positive (red line; $r^2 = -0.411$; *df* 173, $F = 120.9$, $P < 0.0001$) and CGRP-negative (black line; $r^2 = 0.380$; *df* 177, $F = 108.3$, $P < 0.0001$) $\alpha_2\delta$-$1^{WT/WT}$ DRG neurons. (*C*) Intracellular $\alpha_2\delta$-1 density for CGRP-positive (red bars) and CGRP-negative (black/gray bars) DRG neurons from $Ca_V2.2\_HA^{KI/KI}$ $\alpha_2\delta$-$1^{WT/WT}$ (solid bars) and $Ca_V2.2\_HA^{KI/KI}$ $\alpha_2\delta$-$1^{KO/KO}$ (open bars) mice. n = 175, 52, 179, and 72 DRG neurons, respectively, from three sections (one mouse per genotype). ****$P < 0.0001$ (one-way ANOVA and Bonferroni's post hoc comparison of selected conditions). (*D*) Immunostaining for HA (green) in $Ca_V2.2\_HA^{KI/KI}$ $\alpha_2\delta$-$1^{KO/KO}$ DRG neurons, costained with CGRP (*i*) or NF200 (*ii*) (red). Nuclei were stained with DAPI (blue). (Scale bars: 20 μm.) (*E*) Surface $Ca_V2.2\_HA$ intensity in $\alpha_2\delta$-$1^{KO/KO}$ DRG neurons (ratio of perimeter/cytoplasmic staining) for small, medium, and large DRG neurons that are either CGRP-positive (red) or CGRP-negative (black/gray). n = 198, 197, 70, 134, 97, and 109 DRG neurons, respectively, from sections from at least three mice. ****$P < 0.0001$, **$P = 0.0022$ (one-way ANOVA and Sidak's post hoc test). (*F*) Surface $Ca_V2.2\_HA$ intensity (ratio of perimeter/cytoplasmic staining) for small, medium, and large DRG neurons that are either NF200-negative (black/gray) or NF200-positive (red). n = 204, 136, 5, 37, 94, and 168 DRG neurons, respectively, from sections from at least three mice. *$P = 0.0482$ (one-way ANOVA and Sidak's post hoc test). (*G*) Intracellular $Ca_V2.2\_HA$ intensity for CGRP-positive (red) and CGRP-negative (black/gray) $\alpha_2\delta$-$1^{WT/WT}$ (solid bars) and $\alpha_2\delta$-$1^{KO/KO}$ (open bars) DRG neurons. n = 262, 232, 170, and 144 DRG neurons, respectively. Data are from a subset of experiments performed in parallel in which the absolute immunostaining levels are directly comparable. *$P = 0.0308$ (one-way ANOVA and Sidak's post hoc test), ns, not significant. (*H*) Intracellular $Ca_V2.2\_HA$ intensity for NF200-negative (black/gray) and NF200-positive (red) $\alpha_2\delta$-$1^{WT/WT}$ (solid bars) and $\alpha_2\delta$-$1^{KO/KO}$ (open bars) DRG neurons. n = 417, 345, 325, and 299 DRG neurons, respectively. ****$P < 0.0001$ (one-way ANOVA and Sidak's post hoc test).

$Ca_V2.2\_HA$) is recognized by anti-HA antibodies in Western blots of spinal cord tissue from $Ca_V2.2\_HA^{KI/KI}$, but not $Ca_V2.2^{WT/WT}$, mice (Fig. 1*C*).

$Ca_V2.2$ mRNA Levels and Calcium Currents Are Unaltered in $Ca_V2.2\_HA^{KI/KI}$ Compared with $Ca_V2.2^{WT/WT}$ Mice. We next confirmed that the expression of $Ca_V2.2$ did not differ between

$Ca_V2.2\_HA^{KI/KI}$ and $Ca_V2.2^{WT/WT}$ mice. The analyzed expression profiles at 2 and 10 wk postnatally showed that $Ca_V2.2$ mRNA levels were not altered in the $Ca_V2.2\_HA^{KI/KI}$ compared with $Ca_V2.2^{WT/WT}$ mouse brains (Fig. 1*D*).

The properties of calcium channel currents in cultured DRG neurons from 10- to 12-wk-old $Ca_V2.2\_HA^{KI/KI}$ mice were not altered compared with those from $Ca_V2.2^{WT/WT}$ mice, both in terms of current density and voltage-dependent properties (Fig. 1 *E* and *F*). We then examined whether $Ca_V2.2\_HA$ was detectable on the cell surface of cultured DRG neurons from $Ca_V2.2\_HA^{KI/KI}$ mice (Fig. 1*G*). We found $Ca_V2.2\_HA$ to be present on the cell surface particularly of calcitonin gene-related peptide (CGRP)-positive peptidergic nociceptors, to a much greater extent than on isolectin-B4 (IB4)–positive non-peptidergic nociceptors (56.8%, compared with 11.3%; Fig. 1 *G* and *H*). Furthermore, $Ca_V2.2\_HA$ was expressed on only a small

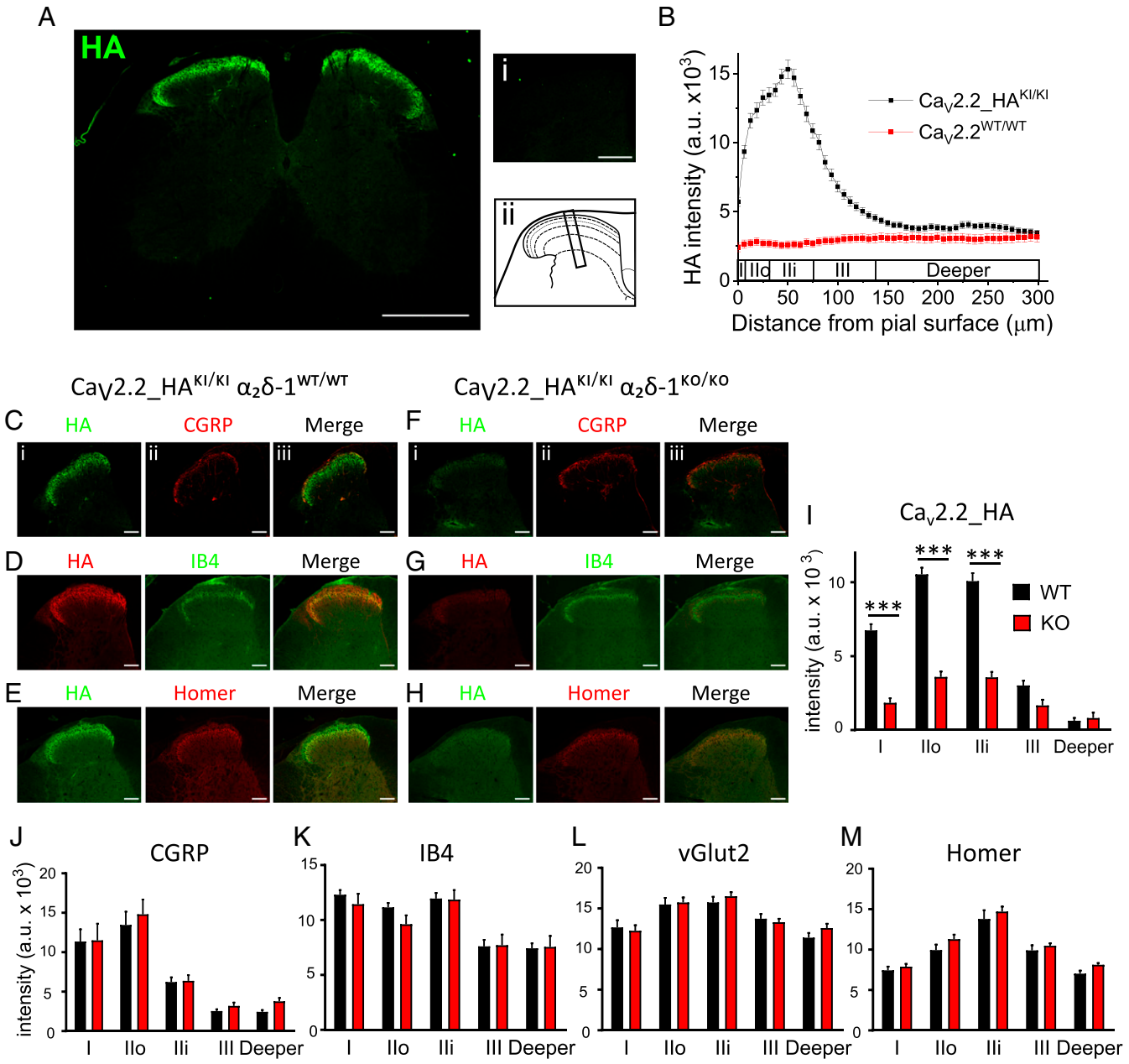

Fig. 4. Effect of $\alpha_2\delta$-1 ablation on distribution of $Ca_V2.2\_HA$ and other synaptic markers in the dorsal horn. (*A*) HA immunostaining (green) in a complete spinal cord section from a $Ca_V2.2\_HA^{KI/KI}$ mouse. (*A*, *Right*) (*i*) Lack of staining in the WT spinal cord, and (*ii*) dorsal horn laminae and ROI perpendicular to the pial surface. [Scale bars: 500 and 200 μm (*i*).] (*B*) $Ca_V2.2\_HA$ intensity (mean ± SEM) in ROIs from the pial surface to 300 μm in the dorsal horn from $Ca_V2.2\_HA^{KI/KI}$ (black squares; $n = 72$ ROIs) and WT (red squares; $n = 36$ ROIs) mice (six ROIs for three experiments for four $Ca_V2.2\_HA^{KI/KI}$ and two $Ca_V2.2^{WT/WT}$ mice). (*C–H*) Dorsal horn HA immunostaining (*Left*, *i*), costained with CGRP (*C* and *F*), IB4 (*D* and *G*), or Homer (*E* and *H*) (*Middle*, *ii*), for $Ca_V2.2\_HA^{KI/KI}$ $\alpha_2\delta$-$1^{WT/WT}$ (*C–E*) and $Ca_V2.2\_HA^{KI/KI}$ $\alpha_2\delta$-$1^{KO/KO}$ (*F–H*) mice. Merged images (*Right*, *iii*). (Scale bars: 100 μm.) (*I–M*) Immunostaining in the dorsal horn from $\alpha_2\delta$-$1^{WT/WT}$ (black bars) and $\alpha_2\delta$-$1^{KO/KO}$ (red bars) mice for $Ca_V2.2\_HA$ (*I*; $n = 72$ and 54 ROIs, respectively), CGRP (*J*; $n = 24$ and 18 ROIs, respectively), IB4 (*K*; $n = 24$ and 18 ROIs, respectively), vGlut2 (*L*; $n = 36$ and 36 ROIs, respectively), and Homer (*M*; $n = 24$ and 18 ROIs, respectively) in laminae I, IIo, Iii, III, and combined deeper layers IV and V. ***$P < 0.001$ (two-way ANOVA and Bonferroni's post hoc test). Data represent mean ± SEM. Box and whisker versions of these plots are in *SI Appendix*, Fig. S7, and details are in *SI Appendix*, Table S2.

proportion of neurofilament 200 (NF200)-positive DRG neurons (77.4% of HA-positive cells were NF200-negative; *SI Appendix*, Fig. S1 *A* and *B*). HA immunostaining was absent from DRG neurons cultured from wild-type mice (*SI Appendix*, Fig. S1*C*).

Cell-Surface Expression of $Ca_V2.2$_HA in DRG Neurons in Vivo. In agreement with the results from cultured DRG neurons, we found that $Ca_V2.2$_HA was clearly present on the cell surface of DRG neuronal somata in sections of ganglia from 10- to 12-wk-old $Ca_V2.2\_HA^{KI/KI}$ mice (Fig. 2 *A*, *i*–*iv*), and absent from $Ca_V2.2^{WT/WT}$ mice (Fig. 2 *A*, *v*). We costained with markers of DRG neuronal subtypes, including CGRP (Fig. 2 *A*, *i*, *ii*, and *v*) and NF200 (Fig. 2 *A*, *iii* and *iv*). Analysis of the ratio of $Ca_V2.2$_HA at the cell perimeter, relative to its cytoplasmic staining, shows that plasma membrane $Ca_V2.2$_HA density is highest on the cell surface of small CGRP-positive DRG neurons (Fig. 2*B*). The small cell-surface $Ca_V2.2$_HA-positive DRG neurons were mainly NF200-negative (Fig. 2*C*). The absolute level of cytoplasmic staining of $Ca_V2.2$_HA was also negatively correlated with the size of DRG neurons (Fig. 2*D*), being higher in small-diameter neurons and in those which are CGRP-positive (Fig. 2*D*) and NF200-negative (Fig. 2*E*).

Knockout of $\alpha_2\delta$-1 Abolishes Cell-Surface Expression of $Ca_V2.2$_HA on DRG Neurons in Vivo. To determine the importance of $\alpha_2\delta$-1 in the cell-surface expression of $Ca_V2.2$_HA, we crossed $Ca_V2.2\_HA^{KI/KI}$ mice with $\alpha_2\delta\text{-}1^{KO/WT}$ mice, and compared $Ca_V2.2\_HA^{KI/KI}$ x $\alpha_2\delta\text{-}1^{KO/KO}$ with their $Ca_V2.2\_HA^{KI/KI}$ x $\alpha_2\delta\text{-}1^{WT/WT}$ littermates. We first confirmed that DRG neurons from $Ca_V2.2\_HA^{KI/KI}$ x $\alpha_2\delta\text{-}1^{WT/WT}$ mice have similar levels of $\alpha_2\delta$-1 to $Ca_V2.2^{WT/WT}$ x $\alpha_2\delta\text{-}1^{WT/WT}$ mice (Fig. 3*A*; quantified in *SI Appendix*, Fig. S2*A*). We found the level of $\alpha_2\delta$-1 to be highest in CGRP-positive small DRG neurons (Fig. 3 *A*–*C* and *SI Appendix*, Fig. S2*A*). As expected, $Ca_V2.2\_HA^{KI/KI}$ x $\alpha_2\delta\text{-}1^{KO/KO}$ DRG neurons show no staining for $\alpha_2\delta$-1 above background (Fig. 3 *A*–*C*).

The effect of genetic ablation of $\alpha_2\delta$-1 on $Ca_V2.2$_HA cell-surface expression was in general very marked (Fig. 3 *D*–*F*). We found that $Ca_V2.2$_HA was not concentrated on the cell surface in $\alpha_2\delta\text{-}1^{KO/KO}$ DRG neurons (Fig. 3*D*), and this was true across all subtypes of DRG neuron examined (Fig. 3 *E* and *F*). Furthermore, there was an increase in mean intracellular $Ca_V2.2$_HA intensity in DRG neurons from $\alpha_2\delta\text{-}1^{KO/KO}$ compared with $\alpha_2\delta\text{-}1^{WT/WT}$ mice, which was found in CGRP-positive DRG neurons (6.9% increase; Fig. 3*G*), and in both NF200-negative and NF200-positive DRG neurons (15.3 and 24.6% increase, respectively; Fig. 3*H*). The elevated intracellular $Ca_V2.2$_HA intensity in $\alpha_2\delta\text{-}1^{KO/KO}$ DRG neurons was also inversely correlated with cell size (*SI Appendix*, Fig. S2*B*).

$Ca_V2.2$_HA Is Localized in the Dorsal Horn of the Spinal Cord. Next, we examined the distribution of $Ca_V2.2$_HA in the spinal cord, and found strong immunoreactivity for the channel subunit in the dorsal horn (Fig. 4*A*). There was very little $Ca_V2.2$_HA in the ventral horn (Fig. 4*A*), and no specific staining in $Ca_V2.2^{WT/WT}$ spinal cord (Fig. 4 *A*, *i*). Taking regions of interest (ROIs) perpendicular to the pial layer (Fig. 4 *A*, *ii*), we found that within the dorsal horn, $Ca_V2.2$_HA was most abundant in superficial laminae I and II (Fig. 4*B*). Here $Ca_V2.2$_HA shares topographic distribution with both the presynaptic markers CGRP, which is present in peptidergic primary afferent terminals in laminae I and II-outer (Fig. 4*C* and *SI Appendix*, Fig. S3*A*), and with IB4, which is present in nonpeptidergic terminals, mainly in lamina II-inner (Fig. 4*D* and *SI Appendix*, Fig. S3*B*). $Ca_V2.2$_HA was also associated with a postsynaptic marker of excitatory synapses, Homer (Fig. 4*E*).

Ablation of $\alpha_2\delta$-1 Reduces $Ca_V2.2$_HA in the Dorsal Horn Without Effect on Other Synaptic Markers. The distribution of $Ca_V2.2$_HA in the dorsal horn was markedly reduced in $\alpha_2\delta\text{-}1^{KO/KO}$ mice (Fig. 4 *F*–*H*), particularly in the superficial layers (Fig. 4*I*). Following subtraction of nonspecific signal found in wild-type $Ca_V2.2$ sections (Fig. 4*B*), the reduction in $Ca_V2.2$_HA was 72.7, 65.9, 64.6, and 44.7% in layers I, II-outer, II-inner, and III, respectively (Fig. 4*I*). This decrease provides clear evidence for the essential role of $\alpha_2\delta$-1 for $Ca_V2.2$ trafficking to the primary afferent presynaptic terminals. In contrast, in the deeper layers of the dorsal horn (laminae IV and V), there was no effect of the ablation of $\alpha_2\delta$-1 on the low level of $Ca_V2.2$_HA present (Fig. 4*I*).

Next, we investigated whether the $\alpha_2\delta$-1–mediated loss of $Ca_V2.2$_HA in the dorsal horn was concomitant with a reduction in density or distribution of synaptic markers, since $\alpha_2\delta$-1 has also been implicated in synaptogenesis (26). In contrast to the marked reduction in $Ca_V2.2$_HA in the absence of $\alpha_2\delta$-1 (Fig. 4*I*), there was no effect of $\alpha_2\delta$-1 ablation on the overall immunostaining intensity or distribution in the dorsal horn of three primary afferent presynaptic markers, CGRP (Fig. 4*J*), IB4 (Fig. 4*K*), and vesicular glutamate transporter-2 (vGlut2) (Fig. 4*L*), and no effect on postsynaptic Homer immunostaining (Fig. 4*M*).

Dorsal Rhizotomy Reduces $Ca_V2.2$_HA in the Dorsal Horn of the Spinal Cord. In light of the marked reduction in $Ca_V2.2$_HA, without loss of synaptic markers, in the dorsal horn of $\alpha_2\delta\text{-}1^{KO/KO}$ mice (Fig. 4*I*), we wished to examine further the extent of its origin in presynaptic primary afferent terminals. To investigate this, we performed unilateral dorsal rhizotomy (Fig. 5*A*). This resulted in a significant reduction of $Ca_V2.2$_HA in the ipsilateral dorsal horn (Fig. 5 *B*–*D*). In the central ROI, the reduction was 52.7% in the superficial layers I and II, and there was also a substantial depletion (by 44.7%) in layers III to V (Fig. 5*D*). Rhizotomy is generally found to be incomplete, as longitudinal fibers remain intact (27). To determine the extent of the rhizotomy, we also examined the level of CGRP, as a marker of loss of presynaptic peptidergic afferents (27). A very similar extensive reduction of CGRP was observed, by 53.1% in layers I and II and 58.6% in layers III to V (Fig. 5 *E* and *F*). The correspondence between the reduction of $Ca_V2.2$_HA and that of CGRP, whose origin is entirely presynaptic in the dorsal horn, confirms the mainly presynaptic localization of the $Ca_V2.2$_HA signal in this region. Following dorsal rhizotomy, there was also a 20.7% decrease of $\alpha_2\delta$-1 in central laminae I and II (*SI Appendix*, Fig. S4), which is expressed both in primary afferents and in intrinsic neurons (20). In contrast, there is no reduction in the NPY signal in the same region (*SI Appendix*, Fig. S4), this peptide being expressed mainly by dorsal horn interneurons (for a review, see ref. 28).

$Ca_V2.2$_HA Subcellular Localization in the Spinal Cord: Effect of $\alpha_2\delta$-1 Ablation. At higher resolution, we observed that $Ca_V2.2$_HA, present in the superficial dorsal horn laminae, was distributed in rosette structures consisting of $Ca_V2.2$_HA puncta surrounding a central core containing vGlut2 and often (but not always) associated with either CGRP (*SI Appendix*, Fig. S5 *A* and *B*) or IB4 (*SI Appendix*, Fig. S5 *C* and *D*), resembling glomerular synapses (29).

To improve resolution of these structures, we then obtained superresolution Airyscan images of $Ca_V2.2$_HA together with vGlut2 and Homer in regions of the dorsal horn in both $\alpha_2\delta\text{-}1^{WT/WT}$ (Fig. 6*A*) and $\alpha_2\delta\text{-}1^{KO/KO}$ mice (Fig. 6*B*). The rosette-shaped clusters of $Ca_V2.2$_HA consisted of groups of four or five puncta (Fig. 6*C*). These puncta may each correspond to individual active zones of primary afferent terminal glomerular synapses, because they are usually organized around a central core containing vGlut2, and also frequently apposed to the postsynaptic marker Homer (Fig. 6*C*).

We found the density of $Ca_V2.2$_HA was markedly reduced in $\alpha_2\delta\text{-}1^{KO/KO}$ dorsal horn (Fig. 6 *B* and *C*), and we quantified the effect on several parameters associated with $Ca_V2.2$_HA puncta (for a method, see *SI Appendix*, Fig. S6). The density of $Ca_V2.2$_HA was reduced in individual clusters of puncta in $\alpha_2\delta\text{-}1^{KO/KO}$

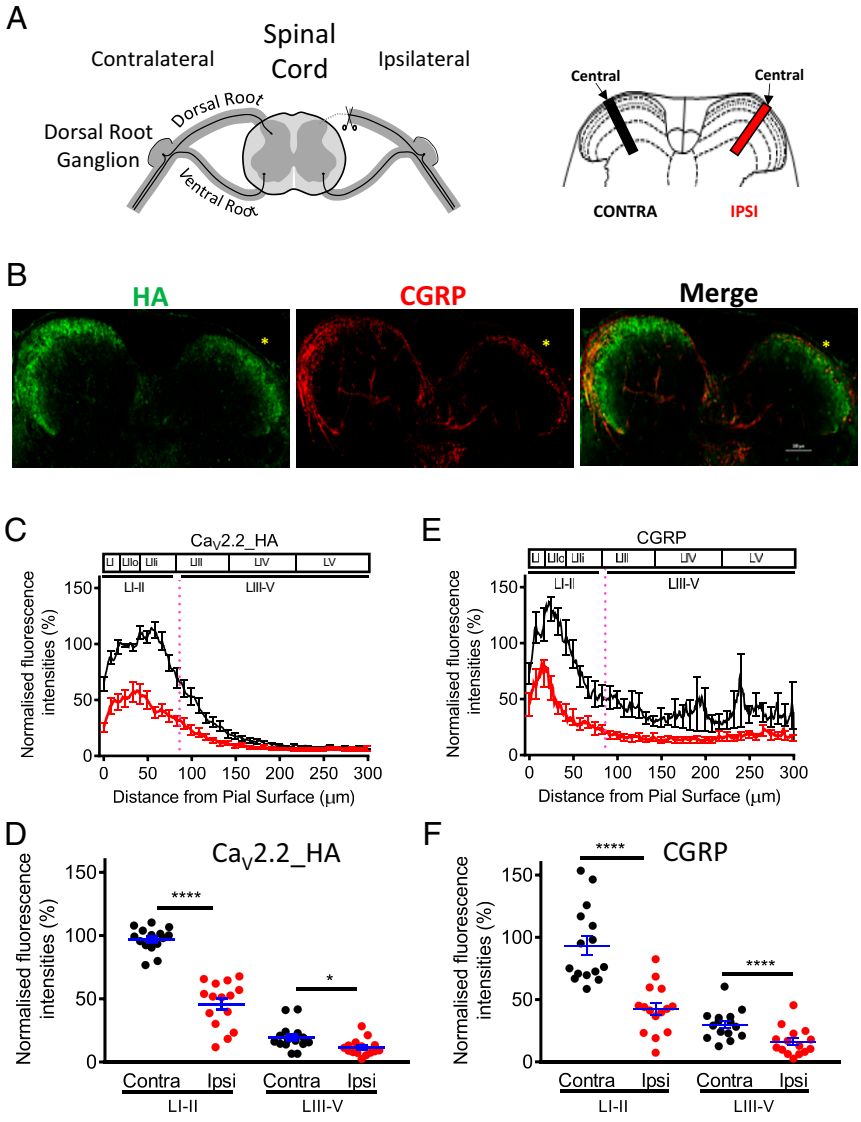

Fig. 5. Effect of dorsal rhizotomy on $Ca_V2.2$_HA distribution in the dorsal horn. (*A*) Diagram of the position of dorsal rhizotomy (*Left*) and central ROIs in the dorsal horn, ipsilateral (ipsi; red) and contralateral (contra; black) to rhizotomy (*Right*). (*B*) Images for $Ca_V2.2$_HA (green; *Left*) and CGRP (red; *Middle*) from a $Ca_V2.2\_HA^{KI/KI}$ mouse following rhizotomy (asterisks). Merged image (*Right*). (*C*) Plot profile of $Ca_V2.2$_HA fluorescence intensity (mean ± SEM of 15 sections, normalized to the average contralateral intensity between 10 and 50 μm) in dorsal horn ROIs, contralateral (black) and ipsilateral (red) to rhizotomy. (*D*) Scatter plots of $Ca_V2.2$_HA intensity (with blue mean ± SEM) for data from *C*, in superficial laminae I and II and in laminae III to V, contralateral (black circles) and ipsilateral (red circles) to rhizotomy. ****$P < 0.0001$, *$P = 0.014$ (paired *t* test). (*E*) Plot profile of CGRP intensity (mean ± SEM of 15 sections, normalized to the average contralateral intensity between 4 and 24 μm) in dorsal horn ROIs, contralateral (black line) and ipsilateral (red line) to rhizotomy. (*F*) Scatter plots of CGRP intensity (with blue mean ± SEM) for data from *E*, in superficial laminae I and II and in laminae III to V, contralateral (black circles) and ipsilateral (red circles) to rhizotomy. ****$P < 0.0001$ (paired *t* test).

dorsal horn, by 47.7% (Fig. 6*D*), but the cluster areas were not significantly affected (Fig. 6*E*). In contrast, neither the area nor the intensity of vGlut2 or Homer clusters was affected by loss of $\alpha_2\delta$-1 (Fig. 6 *D* and *E*). In estimating the pairwise association between $Ca_V2.2$_HA and Homer (Fig. 6*F*), or $Ca_V2.2$_HA and vGlut2 (Fig. 6*G*), we found that the intensity of vGlut2 and Homer in these associated clusters was not affected in $\alpha_2\delta\text{-}1^{KO/KO}$ dorsal horn (Fig. 6 *F* and *G*). However, as expected, the intensity of $Ca_V2.2$_HA in the associated clusters was reduced by 50.0% for $Ca_V2.2$_HA puncta overlapping with Homer (Fig. 6*F*), and by 50.7% for those overlapping with vGlut2 (Fig. 6*G*).

Subcellular Localization of $Ca_V2.2$_HA. To determine the subcellular localization of the $Ca_V2.2$_HA channels, we used preembedding immunogold labeling. For electron microscopic investigation, tissue blocks were taken from the dorsal horn of the spinal cord. Immunoreactivity for $Ca_V2.2$_HA was predominantly found in presynaptic elements, namely on axon terminals of presumed primary afferents (Fig. 7 *A*–*C*). Single or small clusters of immunogold particles were mainly localized to the active zone of boutons, including multiple active zones on individual glomerular boutons (Fig. 7 *B* and *C*), and also appeared at the edge of presynaptic membrane specializations (Fig. 7 *A*–*C*) and along the extrasynaptic plasma membrane (Fig. 7 *A*–*C*) of axon terminals making asymmetrical putative glutamatergic synapses with dendritic shafts and spines of postsynaptic neurons. The specificity of the immunolabeling was confirmed by the absence of immunoreactivity for $Ca_V2.2$_HA in tissues obtained from control animals (Fig. 7*D*).

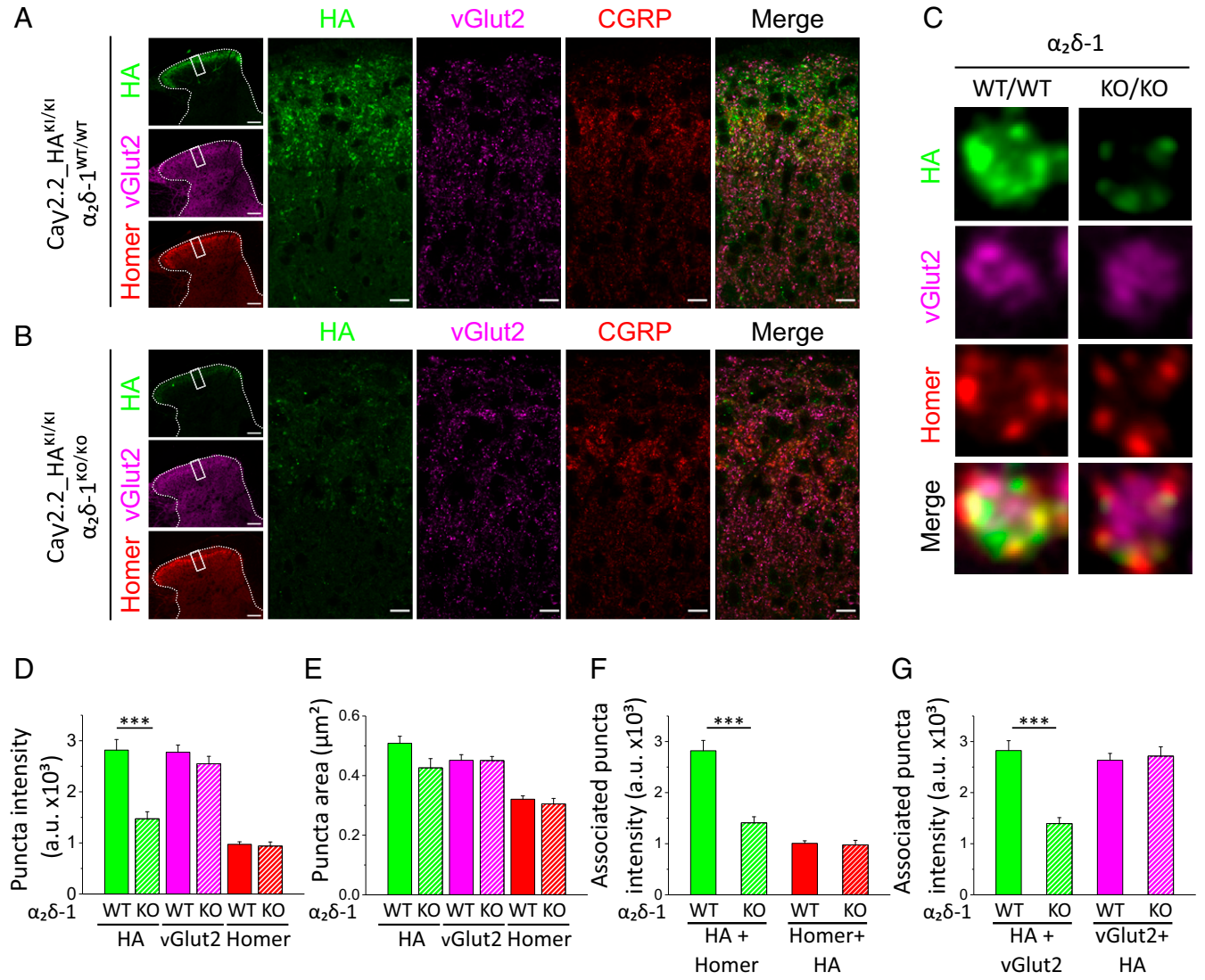

Fig. 6. High-resolution analysis of $Ca_V2.2$_HA puncta in the dorsal horn. (*A* and *B*) Airyscan images from two stitched tiles of 75 × 75 μm across the dorsal horn ROIs (on low-magnification images; *Left*), for $Ca_V2.2$_HA (green), vGlut2 (magenta), Homer (red), and merged, from $Ca_V2.2\_HA^{KI/KI}$ $\alpha_2\delta\text{-}1^{WT/WT}$ (*A*) and $Ca_V2.2\_HA^{KI/KI}$ $\alpha_2\delta\text{-}1^{KO/KO}$ (*B*) sections. (Scale bars: 100 μm and 10 μm in low- and high-magnification images, respectively.) (*C*) Airyscan images (2 × 2 μm) of individual rosette clusters of $Ca_V2.2$_HA puncta from $Ca_V2.2\_HA^{KI/KI}$ $\alpha_2\delta\text{-}1^{WT/WT}$ (*Left*) and $Ca_V2.2\_HA^{KI/KI}$ $\alpha_2\delta\text{-}1^{KO/KO}$ (*Right*) sections. Images (*Top* to *Bottom*) show $Ca_V2.2$_HA (green), vGlut2 (magenta), Homer (red), and merged. (*D* and *E*) Puncta intensity (*D*) and puncta size (*E*) for $Ca_V2.2\_HA^{KI/KI}$ $\alpha_2\delta\text{-}1^{WT/WT}$ (solid bars) and $Ca_V2.2\_HA^{KI/KI}$ $\alpha_2\delta\text{-}1^{KO/KO}$ (hatched bars) for $Ca_V2.2$_HA (green bars), vGlut2 (magenta bars), and Homer (red bars). ***$P = 0.0014$ (Student's *t* test). (*F*) Associated puncta intensity for HA associated with Homer (green bars), and Homer associated with HA (red bars), for $Ca_V2.2\_HA^{KI/KI}$ $\alpha_2\delta\text{-}1^{WT/WT}$ (solid bars) and $Ca_V2.2\_HA^{KI/KI}$ $\alpha_2\delta\text{-}1^{KO/KO}$ (hatched bars). ***$P = 0.0006$ (Student's *t* test). (*G*) Associated puncta intensity for HA associated with vGlut2 (green bars), and vGlut2 associated with HA (magenta bars), for $Ca_V2.2\_HA^{KI/KI}$ $\alpha_2\delta\text{-}1^{WT/WT}$ (solid bars) and $Ca_V2.2\_HA^{KI/KI}$ $\alpha_2\delta\text{-}1^{KO/KO}$ (hatched bars). ***$P = 0.0008$ (Student's *t* test). All data are mean ± SEM of five $Ca_V2.2\_HA^{KI/KI}$ $\alpha_2\delta\text{-}1^{WT/WT}$ and four $Ca_V2.2\_HA^{KI/KI}$ $\alpha_2\delta\text{-}1^{KO/KO}$ ROIs, for 505 and 380; 1,264 and 1,153; or 1,021 and 731 HA and vGlut2 or Homer puncta for $\alpha_2\delta\text{-}1^{WT/WT}$ and $\alpha_2\delta\text{-}1^{KO/KO}$, respectively. Box and whisker versions of plots *D*–*G* are in *SI Appendix*, Fig. S8.

Discussion

In this study, we have been able to visualize native N-type $Ca_V2.2$ channels on the cell surface of neurons in vivo. We have concentrated here on the primary afferent neuronal pathway, because of the importance of $Ca_V2.2$ in synaptic transmission in this system and its therapeutic importance as a drug target (7, 30). We show that $Ca_V2.2$_HA is very strongly expressed on the cell surface, particularly of CGRP-positive small DRG neurons, and this is recapitulated in DRG neurons in culture. In contrast, transcriptional profiling found *Cacna1b* mRNA to be present in similar amounts in IB4-positive and IB4-negative nociceptors, the latter group including CGRP-positive DRG neurons (31). This would agree with the high intracellular $Ca_V2.2$_HA we found in both CGRP-positive and CGRP-negative small DRG neurons. The localization of $Ca_V2.2$_HA in DRG neurons is paralleled by striking expression of $Ca_V2.2$_HA in the dorsal horn of the spinal cord, predominantly in laminae I and II. Here the presynaptic $Ca_V2.2$_HA puncta are associated with the primary afferent markers CGRP, vGlut2, and IB4, present in glomerular primary afferent presynaptic terminals as described previously (29). The $Ca_V2.2$_HA puncta are also adjacent to puncta containing the postsynaptic density protein Homer. The presynaptic localization of $Ca_V2.2$_HA in primary afferents is confirmed through their ablation by dorsal rhizotomy. Furthermore, from the high-resolution immunoelectron-microscopic localization of $Ca_V2.2$_HA, we confirm that these rosette structures formed by the $Ca_V2.2$_HA puncta are likely to represent $Ca_V2.2$_HA in active zones of individual glomerular terminals.

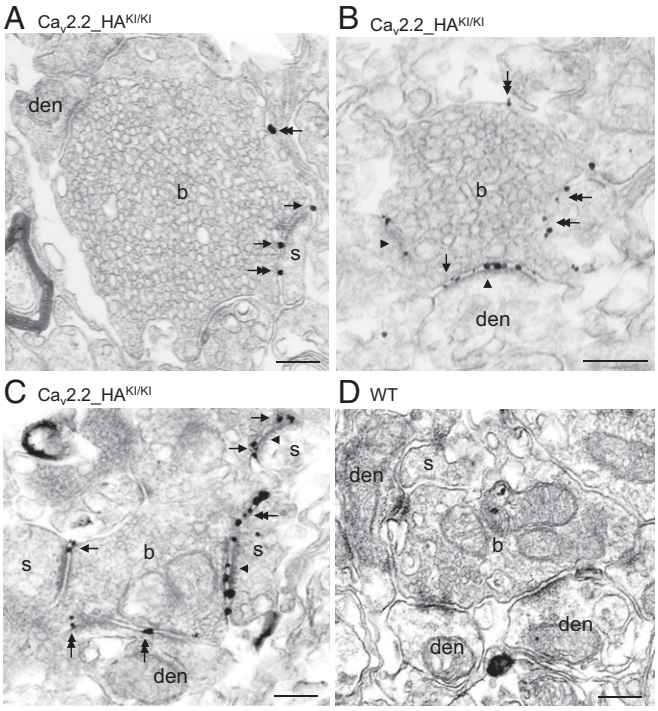

Fig. 7. Subcellular distribution of presynaptic $Ca_V2.2$ channels in putative primary afferent terminals in the dorsal horn of the spinal cord. (*A*–*C*) Electron micrographs showing immunoreactivity for $Ca_V2.2\_HA$ in $Ca_V2.2\_HA^{KI/KI}$ mice detected by the preembedding immunogold method. Immunoparticles labeling HA were observed in the active zone (arrowheads in *B* and *C*) of boutons (b), as well as localized to the perisynaptic (arrows) and extrasynaptic (double arrows) membrane segments of axon terminals making asymmetrical synapses with postsynaptic dendritic shafts (den) and dendritic spines (s). (*D*) No immunolabeling for the channel subunit was detected in tissues from control WT mice. (Scale bars: 200 nm.) Data are from $n = 2$ mice of each genotype.

The $\alpha_2\delta$-1 auxiliary subunit has been shown to be important for calcium channel trafficking in expression systems (13). It plays a major role in pain pathways and is up-regulated following neuropathic injury (17–20, 23). Furthermore, knockout of $\alpha_2\delta$-1 caused a marked delay in the development of neuropathic mechanical hypersensitivity (24), and overexpression of $\alpha_2\delta$-1 mimics features of neuropathic injury (23). In rats, $\alpha_2\delta$-1 is expressed in all DRG neurons with highest expression in small neurons (20), and this distribution is confirmed here, in mice. However, until now it has not been possible to examine the effect of $\alpha_2\delta$-1 on the trafficking of the relevant endogenous N-type channels in vivo.

Our results using $Ca_V2.2\_HA^{KI/KI}$ mice crossed with $\alpha_2\delta$-$1^{KO/KO}$ mice, in which $\alpha_2\delta$-1 is globally ablated, highlight the essential role of $\alpha_2\delta$-1 in directing $Ca_V2.2\_HA$ to the cell surface in DRG neurons and in targeting $Ca_V2.2\_HA$ to presynaptic terminals in the dorsal horn. Accompanying the complete loss of DRG neuronal cell-surface $Ca_V2.2\_HA$, there was also a significant increase in cytoplasmic $Ca_V2.2\_HA$ in CGRP-positive $\alpha_2\delta$-$1^{KO/KO}$ DRG neurons, indicating a defect in cell-surface trafficking.

The calcium currents in DRG neuronal somata in culture are found to be composed of between 20 and 50% N-type current, depending on the species, developmental stage, culture conditions, and subtype of DRG neuron examined (24, 32–35). One comprehensive study showed the proportion of N-type current was about 40% in cultured mouse DRG neurons with a diameter of less than 30 μm, and 20% in those larger than 30 μm (35), which is in agreement with the differential distribution of $Ca_V2.2\_HA$ found here in small DRG neurons. We found previously that in cultured DRG neurons from $\alpha_2\delta$-1 knockout mice the calcium channel current was only reduced by about 30% compared with wild-type DRG neurons, and the N-type current was reduced proportionately (24), which is in contrast to the marked effects of $\alpha_2\delta$-1 knockout on $Ca_V2.2\_HA$ localization described here. It is highly likely that even short-term cultured DRG neurons do not fully represent the in vivo situation, and that rapid changes occur in cell-surface expression of receptors and channels when cells are enzymatically dissociated and maintained in culture, allowing neurite outgrowth (36). Since evoked synaptic currents in laminae I and II are 74% N-type (37), there is likely to be a differential synaptic localization of these channels in vivo.

It has been found that there are other synaptic roles for $\alpha_2\delta$-subunits unrelated to calcium channel function; for example, an association of the extreme C terminus of $\alpha_2\delta$-1 with NMDA receptors has been identified (38). Furthermore, postsynaptic $\alpha_2\delta$-1 has been implicated in central neurons as the binding partner of thrombospondins to promote synaptogenesis induced by this secreted protein family, independent of its role as a calcium channel subunit (26, 39). Thrombospondins alone promote the formation of silent synapses, lacking postsynaptic elements (40). However, we did not detect robust binding of thrombospondin-4 to $\alpha_2\delta$-1 (41). By contrast, in cultured hippocampal neurons, neuroligin was also identified as a binding partner of thrombospondins mediating an increase in the rate of synaptogenesis (42).

Both presynaptic $\alpha_2\delta$-3 (43) and $\alpha_2\delta$-4 (44) have also been implicated in determining synaptic morphology in the auditory system and retina, respectively, although in these cases the synaptic abnormalities resulting from knockout of the respective $\alpha_2\delta$-subunits are likely related to calcium channel dysfunction. In the present study, despite the effect of global ablation of $\alpha_2\delta$-1, which strongly disrupted $Ca_V2.2\_HA$ cell-surface localization, particularly of CGRP-positive small DRG neurons, and markedly reduced presynaptic terminal localization of $Ca_V2.2\_HA$ in the dorsal horn of the spinal cord, we did not observe any reduction in other presynaptic markers of these primary afferents, CGRP, vGlut2, and IB4, or the postsynaptic marker, Homer. At the level of individual synapses, we did not find a reduction in area of $Ca_V2.2\_HA$–positive puncta clusters, but there was a very clear reduction in intensity of $Ca_V2.2$ in each cluster, in the absence of $\alpha_2\delta$-1. This result suggests that, if these puncta represent presynaptic active zones in primary afferent glomerular synapses, $\alpha_2\delta$-1 has not affected the density of synapses in the dorsal horn, despite a large reduction in presynaptic $Ca_V2.2\_HA$ intensity. However, whether there are changes in synaptic morphology will require more detailed examination at the EM level in the future.

Methods

Generation of $Ca_V2.2\_HA$ Epitope-Tagged Knockin Mice. The $Ca_V2.2\_HA$ mouse line was generated by Taconic Artemis in the C57BL/6 background by homologous recombination with the targeting vector, which included the genomic region around exon 13 of the *Cacna1b* gene from clones of a C57BL/6J RPCIB-731 BAC library into which the sequence coding for the 2× HA tag was cloned. The targeting vector also carried the puromycin resistance gene (PuroR) as a positive-selection marker in intron 13 between two Flipper recombination sites and the negative-selection marker thymidine kinase outside the homologous regions. The targeting vector was linearized and transfected into embryonic stem cells. The homologous recombinant clones were isolated by positive and negative selection and injected into blastocysts from BALB/c. Highly chimeric mice were crossed with C57BL/6, and transmission to the germ line was confirmed by black offspring. The positive selective marker was removed by Flipper recombinase after crossing the first generation of knockin mice with Flp deleter transgenic mice. Subsequent backcrossing with wild-type C57BL/6 mice allowed us to select mice without the Flipper transgene and only the 2× HA tag insertion in exon 13. Genotyping PCR was performed with the primers forward, 5′-CACACCAGCATACATGCTCG-3′ and reverse, 5′-TCCAGCCTCACATGCTGC-3′, that bind to the intronic sequences just before and after exon 13 to generate

amplicons of 279 and 345 for the wild-type and knockin allele, respectively. The $Ca_V2.2\_HA^{KI/KI}$ mice showed no difference compared with $Ca_V2.2^{WT/WT}$ mice with respect to body weights (*SI Appendix*, Table S1).

The $\alpha_2\delta$-1 knockout C57BL/6 mouse line described previously (24, 45) was crossed with the $Ca_V2.2\_HA$ knockin mice to generate double-transgenic $Ca_V2.2\_HA^{KI/KI}$ $\alpha_2\delta$-$1^{KO/KO}$ mice. It should be noted that male $\alpha_2\delta$-1 knockout mice on a different genetic background showed a susceptibility to diabetes (46), although we have not noted excessive urination up to 11 wk of age in male double-transgenic mice. Both male and female mice were used in the present study. There was a small reduction of body weight in $Ca_V2.2\_HA^{KI/KI}$ $\alpha_2\delta$-$1^{KO/KO}$ compared with $Ca_V2.2\_HA^{KI/KI}$ $\alpha_2\delta$-$1^{WT/WT}$ mice for both sexes (*SI Appendix*, Table S1).

Mice were housed in groups of no more than five on a 12-h:12-h light:dark cycle; food and water were available ad libitum. All experimental procedures were covered by UK Home Office licenses, had local ethical approval by University College London (UCL) Bloomsbury Animal Welfare and Ethical Review Body, and followed the guidelines of the International Association for the Study of Pain (47).

Additional Methods. Methods for quantitative PCR, synaptosome preparation, immunoblotting, DRG neuronal cultures, electrophysiology, immunocytochemistry in cultured DRG neurons, dorsal rhizotomy, immunohistochemistry, confocal image acquisition and analysis, and preembedding immunoelectron microscopy are included in *SI Appendix*.

Statistical Analysis. Data were analyzed with Prism 5.0 or 7.0 (GraphPad Software) or OriginPro 2015 (OriginLab). Where error bars are shown, they are SEM; "*n*" refers to the number of cells or sections, unless indicated otherwise. Statistical significance between two groups was assessed by Student's *t* test or paired *t* test, as stated. One-way ANOVA and stated post hoc analysis were used for comparison of means between three or more groups. All box and whisker plots show box (25 to 75%) and whisker (10 to 90%) plots with median (line) and mean (+).

ACKNOWLEDGMENTS. We thank Maria Fitzgerald for performing the dorsal rhizotomy surgery, Muftah Dagali for analyzing some of the DRG sections, and Natalie Wernet and Julia Bank for their support with tissue preparation for electron microscopy. This work was supported by a Wellcome Trust Investigator Award (098360/Z/12/Z) (to A.C.D.), and BIOSS-2, Grant A12 and Deutsche Forschungsgemeinschaft FOR 2134 TP4 Grant (both to A.K.).

1. Nowycky MC, Fox AP, Tsien RW (1985) Three types of neuronal calcium channel with different calcium agonist sensitivity. *Nature* 316:440–443.
2. Fox AP, Nowycky MC, Tsien RW (1987) Single-channel recordings of three types of calcium channels in chick sensory neurones. *J Physiol* 394:173–200.
3. Plummer MR, Logothetis DE, Hess P (1989) Elementary properties and pharmacological sensitivities of calcium channels in mammalian peripheral neurons. *Neuron* 2: 1453–1463.
4. Boland LM, Morrill JA, Bean BP (1994) Omega-conotoxin block of N-type calcium channels in frog and rat sympathetic neurons. *J Neurosci* 14:5011–5027.
5. Hirning LD, et al. (1988) Dominant role of N-type Ca^{2+} channels in evoked release of norepinephrine from sympathetic neurons. *Science* 239:57–61.
6. Grantham CJ, Bowman D, Bath CP, Bell DC, Bleakman D (1994) Omega-conotoxin MVIIC reversibly inhibits a human N-type calcium channel and calcium influx into chick synaptosomes. *Neuropharmacology* 33:255–258.
7. Chaplan SR, Pogrel JW, Yaksh TL (1994) Role of voltage-dependent calcium channel subtypes in experimental tactile allodynia. *J Pharmacol Exp Ther* 269:1117–1123.
8. McGivern JG, McDonough SI (2004) Voltage-gated calcium channels as targets for the treatment of chronic pain. *Curr Drug Targets CNS Neurol Disord* 3:457–478.
9. Staats PS, et al. (2004) Intrathecal ziconotide in the treatment of refractory pain in patients with cancer or AIDS: A randomized controlled trial. *JAMA* 291:63–70.
10. Miljanich GP (2004) Ziconotide: Neuronal calcium channel blocker for treating severe chronic pain. *Curr Med Chem* 11:3029–3040.
11. Westenbroek RE, et al. (1992) Biochemical properties and subcellular distribution of an N-type calcium channel α1 subunit. *Neuron* 9:1099–1115.
12. Chi XX, et al. (2009) Regulation of N-type voltage-gated calcium channels (Cav2.2) and transmitter release by collapsin response mediator protein-2 (CRMP-2) in sensory neurons. *J Cell Sci* 122:4351–4362.
13. Cassidy JS, Ferron L, Kadurin I, Pratt WS, Dolphin AC (2014) Functional exofacially tagged N-type calcium channels elucidate the interaction with auxiliary $\alpha_2\delta$-1 subunits. *Proc Natl Acad Sci USA* 111:8979–8984.
14. Macabuag N, Dolphin AC (2015) Alternative splicing in $Ca_V2.2$ regulates neuronal trafficking via adaptor protein complex-1 adaptor protein binding motifs. *J Neurosci* 35:14636–14652.
15. Kadurin I, et al. (2016) Proteolytic maturation of $\alpha_2\delta$ represents a checkpoint for activation and neuronal trafficking of latent calcium channels. *eLife* 5:e21143.
16. Witcher DR, et al. (1993) Subunit identification and reconstitution of the N-type Ca^{2+} channel complex purified from brain. *Science* 261:486–489.
17. Dolphin AC (2012) Calcium channel auxiliary $\alpha_2\delta$ and β subunits: Trafficking and one step beyond. *Nat Rev Neurosci* 13:542–555.
18. Newton RA, Bingham S, Case PC, Sanger GJ, Lawson SN (2001) Dorsal root ganglion neurons show increased expression of the calcium channel alpha$_2$delta-1 subunit following partial sciatic nerve injury. *Brain Res Mol Brain Res* 95:1–8.
19. Luo ZD, et al. (2001) Upregulation of dorsal root ganglion $(\alpha)_2(\delta)$ calcium channel subunit and its correlation with allodynia in spinal nerve-injured rats. *J Neurosci* 21: 1868–1875.
20. Bauer CS, et al. (2009) The increased trafficking of the calcium channel subunit $\alpha_2\delta$-1 to presynaptic terminals in neuropathic pain is inhibited by the $\alpha_2\delta$ ligand pregabalin. *J Neurosci* 29:4076–4088.
21. Brown JP, Dissanayake VU, Briggs AR, Milic MR, Gee NS (1998) Isolation of the [^{3}H]gabapentin-binding protein/alpha$_2$delta Ca^{2+} channel subunit from porcine brain: Development of a radioligand binding assay for alpha$_2$delta subunits using [^{3}H]leucine. *Anal Biochem* 255:236–243.
22. Field MJ, et al. (2006) Identification of the α_2-δ-1 subunit of voltage-dependent calcium channels as a molecular target for pain mediating the analgesic actions of pregabalin. *Proc Natl Acad Sci USA* 103:17537–17542.
23. Li CY, et al. (2006) Calcium channel alpha$_2$delta1 subunit mediates spinal hyperexcitability in pain modulation. *Pain* 125:20–34.
24. Patel R, et al. (2013) $\alpha_2\delta$-1 gene deletion affects somatosensory neuron function and delays mechanical hypersensitivity in response to peripheral nerve damage. *J Neurosci* 33:16412–16426.
25. Müller CS, et al. (2010) Quantitative proteomics of the Cav2 channel nanoenvironments in the mammalian brain. *Proc Natl Acad Sci USA* 107:14950–14957.
26. Eroglu C, et al. (2009) Gabapentin receptor alpha$_2$delta-1 is a neuronal thrombospondin receptor responsible for excitatory CNS synaptogenesis. *Cell* 139:380–392.
27. Chung K, Lee WT, Carlton SM (1988) The effects of dorsal rhizotomy and spinal cord isolation on calcitonin gene-related peptide-labeled terminals in the rat lumbar dorsal horn. *Neurosci Lett* 90:27–32.
28. Todd AJ (2017) Identifying functional populations among the interneurons in laminae I-III of the spinal dorsal horn. *Mol Pain* 13:1744806917693003.
29. Ribeiro-da-Silva A, Pignatelli D, Coimbra A (1985) Synaptic architecture of glomeruli in superficial dorsal horn of rat spinal cord, as shown in serial reconstructions. *J Neurocytol* 14:203–220.
30. Bowersox SS, et al. (1996) Selective N-type neuronal voltage-sensitive calcium channel blocker, SNX-111, produces spinal antinociception in rat models of acute, persistent and neuropathic pain. *J Pharmacol Exp Ther* 279:1243–1249.
31. Chiu IM, et al. (2014) Transcriptional profiling at whole population and single cell levels reveals somatosensory neuron molecular diversity. *eLife* 3:e04660.
32. Scroggs RS, Fox AP (1991) Distribution of dihydropyridine and omega-conotoxin-sensitive calcium currents in acutely isolated rat and frog sensory neuron somata: Diameter-dependent L channel expression in frog. *J Neurosci* 11:1334–1346.
33. Scroggs RS, Fox AP (1992) Calcium current variation between acutely isolated adult rat dorsal root ganglion neurons of different size. *J Physiol* 445:639–658.
34. Desmadryl G, Hilaire C, Vigues S, Diochot S, Valmier J (1998) Developmental regulation of T-, N- and L-type calcium currents in mouse embryonic sensory neurones. *Eur J Neurosci* 10:545–552.
35. Murali SS, et al. (2015) High-voltage-activated calcium current subtypes in mouse DRG neurons adapt in a subpopulation-specific manner after nerve injury. *J Neurophysiol* 113:1511–1519.
36. Emery EC, et al. (2016) In vivo characterization of distinct modality-specific subsets of somatosensory neurons using GCaMP. *Sci Adv* 2:e1600990.
37. Bao J, Li JJ, Perl ER (1998) Differences in Ca^{2+} channels governing generation of miniature and evoked excitatory synaptic currents in spinal laminae I and II. *J Neurosci* 18:8740–8750.
38. Chen J, et al. (2018) The $\alpha_2\delta$-1-NMDA receptor complex is critically involved in neuropathic pain development and gabapentin therapeutic actions. *Cell Rep* 22: 2307–2321.
39. Risher WC, et al. (2018) Thrombospondin receptor $\alpha_2\delta$-1 promotes synaptogenesis and spinogenesis via postsynaptic Rac1. *J Cell Biol* 217:3747–3765.
40. Christopherson KS, et al. (2005) Thrombospondins are astrocyte-secreted proteins that promote CNS synaptogenesis. *Cell* 120:421–433.
41. Lana B, et al. (2016) Thrombospondin-4 reduces binding affinity of [(3)H]-gabapentin to calcium-channel $\alpha_2\delta$-1-subunit but does not interact with $\alpha_2\delta$-1 on the cell-surface when co-expressed. *Sci Rep* 6:24531.
42. Xu J, Xiao N, Xia J (2010) Thrombospondin 1 accelerates synaptogenesis in hippocampal neurons through neuroligin 1. *Nat Neurosci* 13:22–24.
43. Pirone A, et al. (2014) $\alpha_2\delta$3 is essential for normal structure and function of auditory nerve synapses and is a novel candidate for auditory processing disorders. *J Neurosci* 34:434–445.
44. Kerov V, et al. (2018) $\alpha_2\delta$-4 is required for the molecular and structural organization of rod and cone photoreceptor synapses. *J Neurosci* 38:6145–6160.
45. Fuller-Bicer GA, et al. (2009) Targeted disruption of the voltage-dependent calcium channel alpha$_2$/delta-1-subunit. *Am J Physiol Heart Circ Physiol* 297:H117–H124.
46. Mastrolia V, et al. (2017) Loss of $\alpha_2\delta$-1 calcium channel subunit function increases the susceptibility for diabetes. *Diabetes* 66:897–907.
47. Zimmermann M (1983) Ethical guidelines for investigations of experimental pain in conscious animals. *Pain* 16:109–110.